Dissipation at the angstrom scale: Probing the surface and interior of an enzyme

Zahra Alavi[1,2] and Giovanni Zocchi[1,*]

[1]*Department of Physics and Astronomy, University of California Los Angeles, Los Angeles, California 90095, USA*

[2]*Department of Physics and Astronomy, Loyola Marymount University Los Angeles, Los Angeles, California 90095, USA*

(Received 20 July 2017; revised manuscript received 22 September 2017; published 10 May 2018)

Pursuing a materials science approach to understanding the deformability of enzymes, we introduce measurements of the phase of the mechanical response function within the nanorheology paradigm. Driven conformational motion of the enzyme is dissipative as characterized by the phase measurements. The dissipation originates both from the surface hydration layer and the interior of the molecule, probed by examining the effect of point mutations on the mechanics. We also document changes in the mechanics of the enzyme examined, guanylate kinase, upon binding its four substrates. GMP binding stiffens the molecule, ATP and ADP binding softens it, while there is no clear mechanical signature of GDP binding. A hyperactive two-Gly mutant is found to possibly trade specificity for speed. Global deformations of enzymes are shown to be dependent on both hydration layer and polypeptide chain dynamics.

DOI: 10.1103/PhysRevE.97.052402

I. INTRODUCTION

Enzymes are structured but deformable macromolecules. Assuming a specific conformation allows the enzyme to catalyze a specific chemical reaction, while deformability confers the ability to operate as molecular machines. In their natural cycle, enzymes are deformed by binding of the reactants ("substrates") and unbinding of the products [1,2]—a property which may have coevolved with catalytic ability [3]. Deformability is, however, a more general materials property of the folded protein, and enzymes can be deformed—and their activity modulated—by perturbations other than ligand binding [4,5]. This materials science aspect can be advantageously investigated by nanorheology, a technique that can probe the mechanics of the folded enzyme with subangstrom (sub-Å) resolution in the deformation, in the frequency range (10 Hz–10 kHz) relevant for the large conformational motion of these molecules [6,7]. Nanorheology is essentially a traditional rheology experiment, where one imposes an oscillatory stress and measures the resulting strain, except that the material between the plates of the rheometer is one or a few molecules, and one of the "plates" is correspondingly shrunk to the nanometer scale. Figure 1 explains the concept: the enzyme molecules tether 20-nm-size Au nanoparticles to a gold surface which forms the bottom of a fluid chamber; the top is formed by a second gold electrode in a parallel plates capacitor configuration. An AC electric field produces a sinusoidal force on the GNPs, since the latter are charged due to surface chemistry modifications. Thus, a sinusoidal stress is exerted on the enzymes. The oscillation of the GNPs in the direction orthogonal to the plate is measured by evanescent wave scattering, corresponding to an ensemble average over $\sim 10^8$ GNPs in this particular apparatus. The nanometer-size thermal motion of each GNP adds incoherently to the scattered intensity and so averages to zero, while the collective oscillation driven by the electric field adds coherently and can be measured with sub-Å resolution. The nanorheology setup is essentially an ensemble of $\sim 10^8$ synchronous nanoscale rheometers with ensemble averaged readout.

With this instrument, the internal rheology of one particular enzyme—guanylate kinase (GK)—has been investigated in some detail. Before proceeding, we stress that "the enzyme" means the folded polypeptide chain plus the hydration layer at its surface. The hydration layer is an integral, indispensable part of the molecule [8]; without it, "the enzyme" is a different object: in particular, its functionality and dynamics is impaired. Unlike individual spectroscopic techniques, which deal with either the polypeptide chain or the hydration water, nanorheology deals with both. The gold surfaces exert a stress on the hydration layer, which exerts a stress on the polypeptide chain. The gold has, of course, its own hydration layer, which is also an interesting object of study [9]. The dynamics seen by nanorheology is the dynamics of the whole system: polypeptide chain plus hydration layer. Now we summarize the results obtained previously. It was discovered that the dynamics of angstrom-size deformations of the enzyme is viscoelastic: elastic at "high" frequency, viscous flow like at "low" frequency [10]. High and low refers to a characteristic corner frequency $\omega_c \sim 100$ rad/s well defined in the experiments. The system is nonlinear in that, for example, the characteristic frequency ω_c depends on the amplitude F_0 of the applied force [11]. Indeed, at fixed forcing frequency ω and for increasing F_0, the system undergoes an abrupt dynamic softening transition at a critical deformation amplitude $x_c \sim 1$ Å (rms) [12]. This value depends on ω [13]. A viscoelastic transition implies dissipative dynamics [7,14]; interpreting the corner frequency ω_c as a ratio of an elastic and a dissipative parameter: $\omega_c = \kappa/\gamma$ one finds indeed that the enzyme is effectively very viscous [10].

The purpose of this study is to examine more closely this molecular scale dissipation. We use the same GK enzyme as

*zocchi@physics.ucla.edu

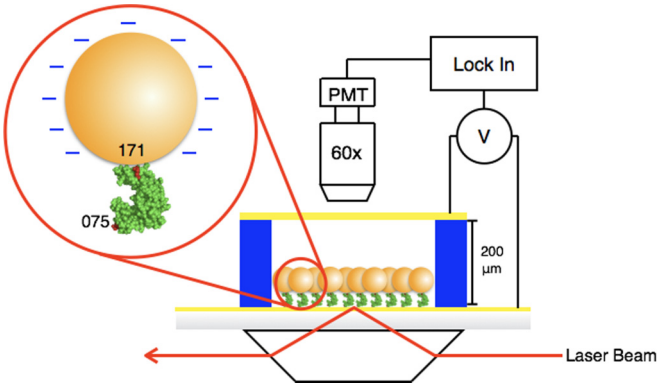

FIG. 1. Nanorheology setup, showing the flow chamber with enzyme-tethered GNPs, the parallel plates capacitor geometry used for mechanical excitation, and the evanescent wave scattering optics used for read out.

in previous studies. First we introduce, for the first time with this instrument, the measurement of the phase φ (between applied force and resulting deformation), which is a direct measure of dissipation. Namely, for a linear system, an applied force $F(t) = F_0\cos(\omega t)$ would result in a deformation $x(t) = x_0\cos(\omega t + \varphi)$; the work done by the force over one cycle, which is the dissipation, is

$$W = \int_0^{2\pi/\omega} F\dot{x}\,dt = -\int_0^{2\pi/\omega} dt\,F_0x_0\omega\cos(\omega t)\sin(\omega t+\varphi) = \pi F_0x_0\sin(-\varphi). \quad (1)$$

For a nonlinear response, defining the dissipation is more delicate, but it is still true that $\varphi = 0$ corresponds to completely nondissipative, and $\varphi = -\pi/2$ to completely dissipative, behavior, as explained, for example, in Ref. [14]. In the general nonlinear case, the phase φ is defined by multiplying the signal by synchronous sines and cosines, averaging, and taking the ratio:

$$x_r = \int_0^{2\pi/\omega} dt\,x(t)\cos(\omega t), \quad x_i = \int_0^{2\pi/\omega} dt\,x(t)\sin(\omega t), \quad \tan(\varphi) = x_i/x_r. \quad (2)$$

We will see that, similar to macroscopic rheology, for this molecular system the measurement of the phase also offers a consistent physical characterization, of the viscoelastic dynamics on the one hand, and of perturbations applied to the system on the other hand. In some cases, binding isotherms for ligands binding to the enzyme can be obtained from the phase signal instead of (or in addition to) the amplitude signal. Next, we ask the following general question: Does the dissipation in the system originate mainly from the surface of the molecule, which includes the hydration layer, or from the interior, or both?

The role of the hydration layer in protein dynamics has, of course, been investigated before. It is clear that the hydration layer is an integral part of the protein [8]: Without hydration layer, the molecule is a totally different object as far as dynamics and functionality. This is not surprising: Unlike bulk materials, the physical properties of nanoparticles derive both from the surface and the interior. For a globular protein the size of GK, more than half the amino acid residues are at the surface of the molecule, and the "surface" comprises a dynamic network of hydrogen bonds between and among water molecules in the hydration layer and residues at the surface. The coupling between hydration layer and polypeptide chain dynamics has been investigated in a long series of experiments by Frauenfelder and collaborators [15–17] and others [18–20]. Fluctuations in the hydration layer can be measured, for example, by dielectric spectroscopy; fluctuations in the polypeptide chain by neutron and x-ray scattering, by femtosecond fluorescence spectroscopy, and, in the case of haemoglobin, by Mossbauer spectroscopy of the Fe atom in the heme group. Fast water dynamics in the hydration layer is also measured by nuclear magnetic resonance [21] and Overhauser dynamic nuclear polarization [20,22]. Summarizing a wealth of experimental data, and following Refs. [8,18], we may say that the hydration shell fluctuations are strongly coupled to polypeptide chain fluctuations.

The above experiments probe phenomena at timescales from nanoseconds to picoseconds. One interesting feature of nanorheology is that it probes deformation dynamics of the hydration layer and the folded polypeptide structure at timescales from 100 ms to 100 μs, which are also the timescales of large conformational motion induced by ligand binding, i.e., the timescales of the mechanochemical cycle of enzymes. In fact, the nanorheology "cycle" is not so very different from a binding-unbinding cycle. There are two hydration layers: one at the enzyme's surface and one at the gold's surface. When gold and enzyme are pressed together, the hydration layers are compressed and possibly partially expelled from a small surface of contact, and the polypeptide structure also deforms; when gold and enzyme are pulled apart, the hydration layers and molecule shape go back to their previous state. Ligand binding similarly perturbs the hydration layers at the surface of contact between interacting molecules.

We now proceed to the next question: Does the dissipation measured by nanorheology originate from the surface or the interior of the enzyme? Previously we showed that chemically perturbing the hydration layer has a big effect on the measured dissipation [23]. Here we study the effect of point mutations in the interior of the molecule, specifically, a one-Gly substitution (mutant B1) and a two-Gly substitution (mutant C1). The location of the mutations was chosen in a region that undergoes high strain during the enzymatic cycle, based on the structures of the open (apo) and closed (GMP bound) conformations of the enzyme [24]. There is a readily observable effect on the enzymatic activity, the B1 mutant being roughly 10 times slower than the wild type (WT), while C1 is roughly 10 times *faster*, in itself a surprising result. However, summarizing the results of many experiments detailed below, we find that the effect of the point mutations on the mechanics measured by nanorheology is relatively small. There is also no dramatic effect on the binding constants of substrates and products, which is perhaps not surprising since the mutations are far from the active site. Summarizing our main results: We introduce the measurement of the phase of the response function and further characterize the dissipation occurring during the driven angstrom-size deformations of the system. The results reaffirm the importance of the hydration layer in enzyme dynamics, but, for the first time, on the slow timescales of order the inverse rate

for large conformational motion. We find subtle mechanical differences between the WT and the C1 (2-Gly) mutant, which is a 10 times faster enzyme. The internal dissipation appears increased for C1, that is, the mutant is more resistive to large conformational motion. Finally, for the specific enzyme of this study, we document the changes in stiffness of the enzyme upon binding the four main ligands: GMP, ATP, GDP, ADP. In doing so we found indications that the fast (C1) mutant has an increased propensity to bind GMP *in the ATP binding site*, possibly an example of trading specificity for speed [25,26].

II. RESULTS

We present two kinds of measurements: frequency scans, where the frequency of the applied sinusoidal force is varied (at fixed amplitude of the force), and "concentration scans," or binding curves, where the concentration of a ligand (e.g., GMP) is varied, while the response is measured at a fixed frequency (and fixed force amplitude). For both cases, we measure amplitude and phase of the response. The light intensity from the scattering setup is modulated at the forcing frequency, reflecting the synchronous oscillation of the GNPs; this signal, acquired with a photomultiplier, is combined with the reference forcing signal by a lock-in amplifier (Fig. 1), which performs the operations Eq. (2), yielding the real and imaginary parts of the response, x_r and x_i, from which the amplitude $x = \sqrt{x_r^2 + x_i^2}$ and phase $\varphi = \arctan(x_i/x_r)$ are calculated. The optical readout is by evanescent wave scattering [6,27] combined with the plasmon resonance of the gold strip and gold nanoparticles [28,29]. Using a He-Ne laser (wavelength 633 nm) for illumination, the evanescent wave scatters directly off the GNPs, but it also excites the plasmon resonance in the 30-nm-thick gold strip, which excites the plasmon resonance in the GNPs in a distance-dependent manner. The result is a much (∼500 times) larger scattered intensity and ∼6-fold larger distance sensitivity compared to scattering off resonance using an Ar (wavelength 488 nm) laser [29]. We have calibrated the distance sensitivity of this setup (the relation between modulation of the scattered intensity and actual displacement of the GNPs) by comparing scattering on resonance with scattering off resonance, which can be calculated; details are reported in Ref. [29]. However, the force is not calibrated in the experiments, though we have shown that it is proportional to the applied voltage [10]. We choose the latter to operate in the regime of large but reversible deformations, which for this molecule and setup means root-mean-square deformation amplitudes $x < 3$ Å or so. Under these circumstances the enzymes in the apparatus are in their native, functional state; for instance, binding constants for the substrates obtained by nanorheology are essentially the same as for the enzyme in solution [29].

In the following we will often use, in discussing the data, the simplest model of visco-elasticity, which is the Maxwell model. While it is a linear model, it describes *the frequency dependence* of the deformation amplitude measured in the experiments remarkably well [11]. We therefore summarize it here. The equation of motion for the model is

$$\dot{x} = \frac{1}{\kappa}\dot{F} + \frac{1}{\gamma}F, \tag{3}$$

where $x(t)$ is the deformation, $F(t)$ the applied force, κ the elastic parameter, and γ the dissipation parameter. With an applied sinusoidal force $F(t) = F_0\cos(\omega t)$ the response is

$$x(t) = \frac{F_0}{\omega\gamma}\left[\sin(\omega t) + \frac{\omega}{\omega_c}\cos(\omega t + \varphi)\right], \tag{4}$$

where the amplitude and phase are

$$x_0 = \frac{F_0}{\omega\gamma}\sqrt{1 + \left(\frac{\omega}{\omega_c}\right)^2}, \quad \varphi = -\arctan\left(\frac{\omega_c}{\omega}\right). \tag{5}$$

The corner frequency $\omega_c = \kappa/\gamma$ separates elastic ($\omega \gg \omega_c$) from viscous ($\omega \ll \omega_c$) behavior. The work done by the force F over one cycle, which is the energy dissipated over one cycle, is

$$W = \int_0^{2\pi/\omega} F\dot{x}\,dt = \int_0^{2\pi/\omega} dt\,\frac{F_0^2}{\gamma}\cos^2(\omega t) = \frac{\pi F_0^2}{\omega\gamma}, \tag{6}$$

the same as for a pure flow, since this is a linear model. This work can be written in terms of different combinations of the thermodynamic variables $F_0, x_0, \varphi, \omega$; for example,

$$W = \pi F_0 x_0 \sin(-\varphi), \tag{7}$$

which is valid for any linear response function, not just the Maxwell model. But also,

$$W = \pi\gamma\,\frac{x_0^2\omega}{1 + (\omega/\omega_c)^2} = \frac{\pi}{2}\kappa x_0^2\sin(-2\varphi). \tag{8}$$

These forms are specific to the Maxwell model; they show that, *at fixed* x_0, the dissipation is maximum for $\omega = \omega_c$ (and $\varphi = -\pi/4$).

We now examine the measurements. Figure 2 shows a representative example of frequency scan for the WT.

Let us first concentrate on the circles. In Fig. 2(a) we have the amplitude of the deformation, x_0. It shows the viscoelastic response documented before [10,11]: $x_0 \sim$ const. (independent of ω) above a corner frequency ω_c, and $x_0 \sim 1/\omega$ below ω_c. The line is a fit with the form for x_0 given in Eq. (5), returning the value $\omega_c = 163$ rad/s (note that the experimental data are plotted as a function of frequency $\nu = \omega/2\pi$ in cycles/s). In Fig. 2(b) we have the phase φ, for the same measurements. Qualitatively, it confirms that the dynamics is viscoelastic: nondissipative for $\omega \gg \omega_c$ (φ approaches zero), dissipative for $\omega \ll \omega_c$ (φ approaches $-\pi/2$). The line is a fit with the Maxwell model prediction in Eq. (5), returning the value $\omega_c = 213$ rad/s. The discrepancy between the values of ω_c obtained from Figs. 2(a) and 2(b), which is systematic, indicates that the Maxwell model Eq. (3) describes the measurements only partially. Discrepancies are more evident in the phase plots, because the corresponding fits are one parameter fits. In Fig. 2(c) we replot the same data, but plotting the quantity $\pi x_0 \sin(-\varphi)$ versus ω. For any linear response system, including the Maxwell model, this quantity is equal to W/F_0; see Eq. (7). In the Maxwell model, this same quantity is proportional to $1/\omega$, because from Eq. (6),

$$\frac{W}{F_0} = \frac{\pi F_0}{\gamma}\frac{1}{\omega}. \tag{9}$$

The line in Fig. 2(c) is a fit using the form of the right-hand side of Eq. (9), returning the value $(\pi F_0/\gamma) = 67$ Å rad/s. We

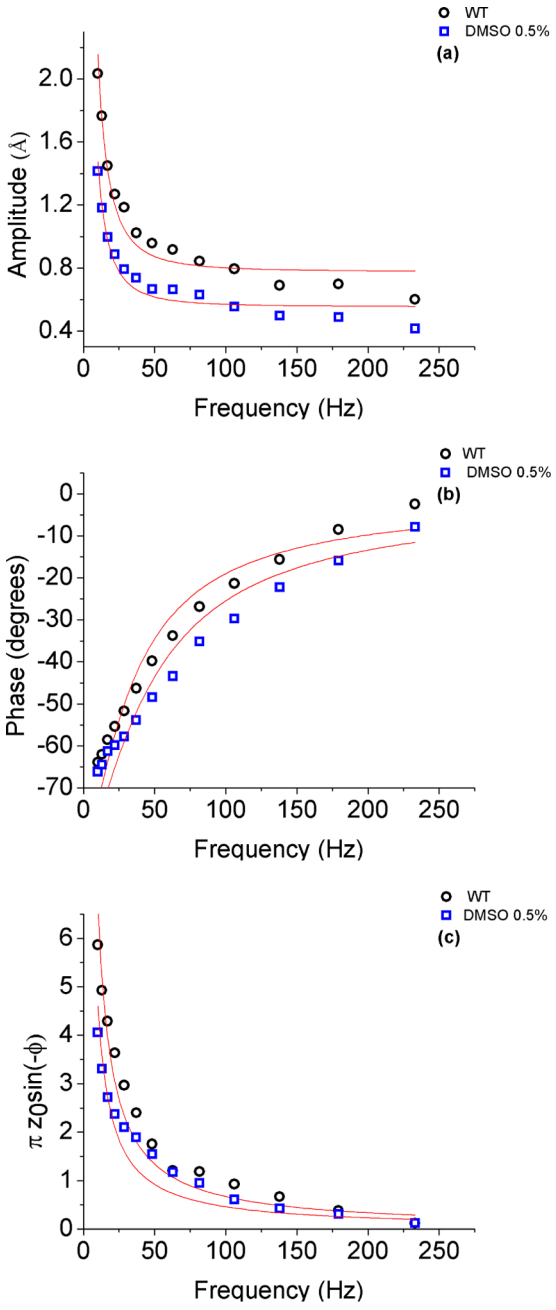

FIG. 2. Frequency scan showing the mechanical response of the wild type (WT), under our standard conditions (in SSC/3, 50 mM total ionic strength, pH = 7.0; circles) and with the addition of 0.5 % DMSO (a kosmotropic agent affecting the hydration layer; squares). The data are obtained from the same sample. (a) RMS amplitude x_0 of the response (in Å) vs. frequency $\nu = \omega/2\pi$ (in cycles/s). The lines are fits with Eq. (5), returning the values $F_0/\gamma = 20$ Å/s, $\omega_c = 163$ rad/s (circles) and $F_0/\gamma = 14$ Å/s, $\omega_c = 153$ rad/s (squares). (b) Phase φ of the response [defined operationally in Eq. (2)] vs. frequency. The lines are one-parameter fits with Eq. (5) and show that the Maxwell model Eq. (3) does not quite describe the system. (c) This plot is a measure of dissipation. For the same data as (a) and (b), the quantity $\pi x_0 \sin(-\varphi)$ is plotted (in Å) vs. frequency. For a linear system this quantity would be equal to W/F_0 [Eq. (7)], where W is the energy dissipated per cycle and F_0 is the amplitude of the applied force. For the Maxwell model, this quantity is proportional to $1/\omega$ [Eq. (6)]; the lines are one-parameter fits with the form const./ω.

see that there is internal consistency between the measurements of the amplitude x_0 and the phase φ, and that both quantities roughly follow the frequency dependence of the Maxwell model of viscoelasticity. We therefore feel justified in interpreting the measured quantity $\pi x_0 \sin(-\varphi)$, for fixed F_0, as a measure of the dissipation according to Eq. (7). Figure 2(c) then shows that, at constant F_0, the system is dissipative at low frequency and non dissipative at high frequency. This is, of course, completely different from a damped spring, which is nondissipative at low frequency.

Let us now discuss the data plotted as squares in Fig. 2. They represent the same sample as the circles, where DMSO (Dimethyl sulfoxide) 0.5% (70 mM) has been added to the buffer. DMSO is classified as an order inducing (kosmotropic) agent with respect to the hydration layer of hydrophilic solutes [30–32]; at the small concentrations we are using, its effect on the physical properties of bulk water (viscosity, dielectric constant) is negligible. On the contrary, we reported before that its effect on the "stiffness" of the hydration layer as measured by nanorheology is significant [23]. The squares in Fig. 2(a) confirm that conclusion: for the same applied force, the presence of 0.5% DMSO causes the deformation amplitude to drop by a factor 0.7. The new measurements of the phase [Fig. 2(b)] show that the effect can be thought of as making the system more viscous: the phase decreases as DMSO is added at constant force. Figure 2(c) shows that, in terms of the dissipation parameter γ of the Maxwell model, the dissipation measurements roughly agree with the amplitude measurements in finding an increase in γ by a factor 1.46 with DMSO present. Namely, interpreting the prefactor in the $1/\omega$ fits according to Eq. (9), we find $\pi F_0/\gamma = 67$ Å rad/s for the circles, and $\pi F_0/\gamma_{\rm DMSO} = 46$ Å rad/s for the squares, giving $\gamma_{\rm DMSO}/\gamma = 1.46$.

Since DMSO is known to affect the hydration layer but is unlikely to penetrate the interior of the protein and affect the structure (for instance, DMSO causes a small *increase* in enzymatic speed for this enzyme [23]), we conclude that a large part of the dissipation measured by nanorheology comes from the hydration layer, confirming the results in Ref. [23].

Having established that the surface of the molecule, which includes the hydration layer, is very important for the mechanics measured in the experiments, we now turn to the question of how important is the interior of the molecule. We prepared two different mutants of GK, substituting Ala 176 with a Gly (Ala176Gly: mutant B1) and substituting Ala 176 and Ala 175 with Gly (mutant C1).

Glycine is the smallest amino acid, and it was thought that Gly substitutions in the interior would be the least disruptive of the overall structure. Indeed, both mutants are enzymatically active, as we see below. The location of the mutations was chosen in a region that undergoes large strains during the open to closed transition of the enzymatic cycle driven by GMP binding. Namely, we produced a strain map by comparing the open (apo) and closed (GMP bound) x-ray structures of the enzyme [24,33] (the corresponding PDB structures are 1ZNX for the closed state and 1ZNW for the open state). We defined a simple measure of "strain" according to

$$S(n) = \sum_m \left|\Delta_{nm}^{(o)} - \Delta_{nm}^{(c)}\right| / \Delta_{nm}^{(o)}, \qquad (10)$$

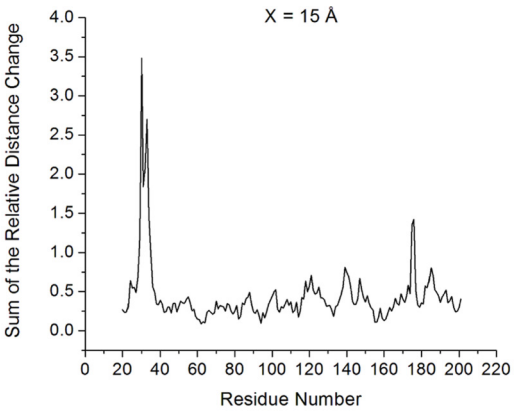

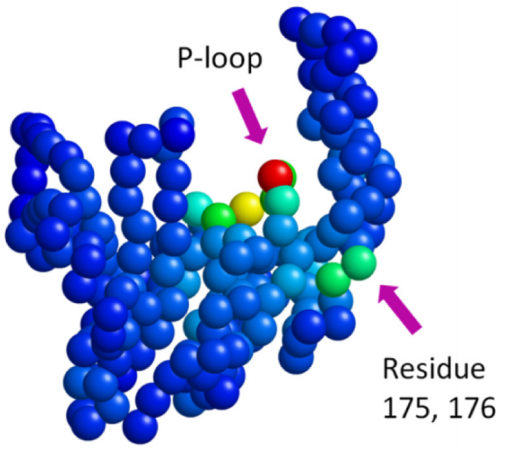

FIG. 3. (a) Map of the relative distance change of Cα atoms of GK from the open to the closed states; the distance change is averaged over Cα atoms along the chain within a cutoff X ($X = 15$ Å for this graph). Two major peaks appear in this strain map: one for residues 29–35, which is the p-loop, and another for residues 175–176, the region often called "hinge." The same features appear when varying the cutoff X from 8 to 18 Å. (b) Color map of the graph in (a) painted on the GK structure (only Cα atoms are shown), with increasing "strain" from blue to red. The structures used for this map were PDB 1ZNX (closed state) and 1ZNW (open state).

where $\Delta_{nm}^{(o)}$ is the distance between the Cα carbons of residues n,m in the open structure, $\Delta_{nm}^{(c)}$ is the same for the closed structure, and the sum is over neighbors within a cutoff distance $\Delta_{nm}^{(o)} \leqslant X$. The resulting S for $X = 15$ Å is shown in Fig. 3, plotted versus residue number n. This measure does pick out interesting regions of high strain, namely the so-called p-loop around residue 30 (a conserved sequence essential for catalysis in kinases which experiences a large conformational change from the open to the closed state [34]) and one more spot around residue 175. The latter is the location chosen for the mutations, as it is distant from the active site.

Figure 4 shows measurements of the enzymatic activity of the two mutants B1 (Ala176Gly) and C1 (Ala176Gly, Ala175Gly) compared to the WT. The bar graph shows the (initial) speed (on a log scale) of the enzymatic reaction under substrate conditions optimal for the WT (initial concentration of GMP 1 mM and ATP 2 mM). For all measurements, enzyme

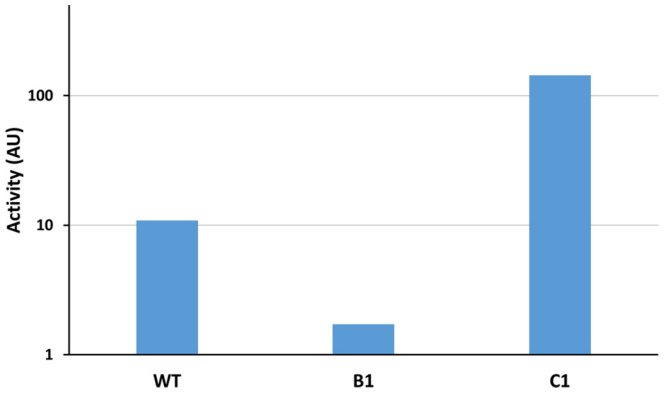

FIG. 4. Comparison of the enzymatic activity (plotted on a log scale) of the WT and the two mutants. The quantity plotted is the initial speed of the enzymatic reaction, measured with a pyruvate-NADH coupled enzymatic assay (see Sec. IV). Conditions were the same for all measurements (optimal conditions for the WT, [GMP] = 1 mM, [ATP] = 2 mM), the nominal enzyme concentration being determined with the Bradford assay.

concentration was the same, as measured by the Bradford assay on the stock solutions. We see that the two-Gly mutant C1 is ∼10 times faster than the WT, while B1 is ∼10 times slower. Comparing B1 and C1, a single Gly substitution in a "high strain" region away from the active site is found to modulate the reaction speed by a factor 100. Also noteworthy is the surreptitious discovery of the two-Gly mutant, which is *faster* than the WT. Since we tend to view biological machinery as "optimized," it is natural to ask what tradeoff the C1 mutant may represent. We come back to this question later.

We have also obtained (rough) GMP and ATP titration curves of the enzymatic speed for the mutants, which show that any difference in Michaelis-Menten constants between the mutants and the WT, if present, is small. The factors of 10 in speed are due, within the Michaelis-Menten description, to the rate of the chemical reaction $k_{\rm cat}$, and not to differences in substrates binding affinities. This conclusion is consistent with the measurements of dissociation constants K_d by nanorheology which we discuss later for substrates and products. These measurements show that the speed differences are also not due to differences in binding affinity of the products.

Looking for mechanical signatures distinguishing the mutants from the WT, Figs. 5 and 6 show representative frequency scans for B1 and C1, to be compared with Fig. 2. Comparing different mutants, which must be done by comparing different samples, is more difficult than comparing different solvent [23] or temperature [7] conditions, which can be done on the same sample. The reason is the sample to sample variability in the effective proportionality constant between the applied voltage and the actual force on the enzymes, which is not calibrated in the experiments. Nonetheless, some trends emerge, especially after averaging over several samples, as we see below.

In both Figs. 5 and 6, the line in panels (a) and (b) is a fit with Eq. (5). The value of F_0/γ obtained from plotting amplitude of response in panel (a) for both figures is $\simeq$20 Å/s, which agrees with the corresponding dissipation plots in panels (c). The line in panels (c) is a fit with Eq. (9). Both figures give similar values for ω_c extracted from the amplitude plots, namely

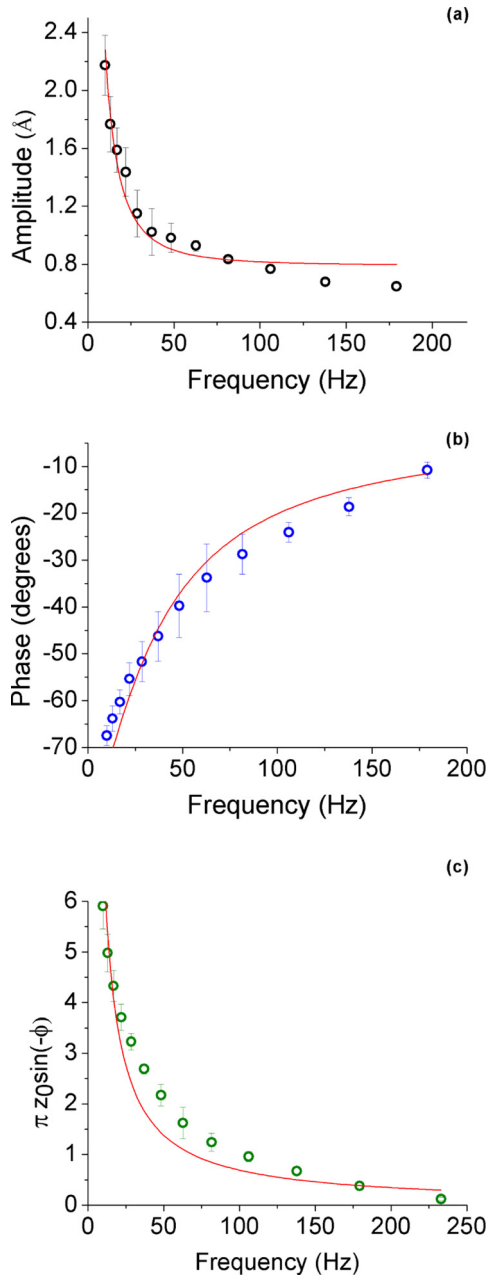

FIG. 5. Representative nanorheology frequency scans for the mutant C1. Panels (a), (b), and (c) show, respectively, the root-mean-square amplitude of the mechanical response, the phase, and the dissipation [the quantity $\pi x_0 \sin(-\varphi)$]. The frequency is $\nu = \omega/2\pi$, in cycles/s. The lines are fits with the Maxwell model predictions Eqs. (5) and (9).

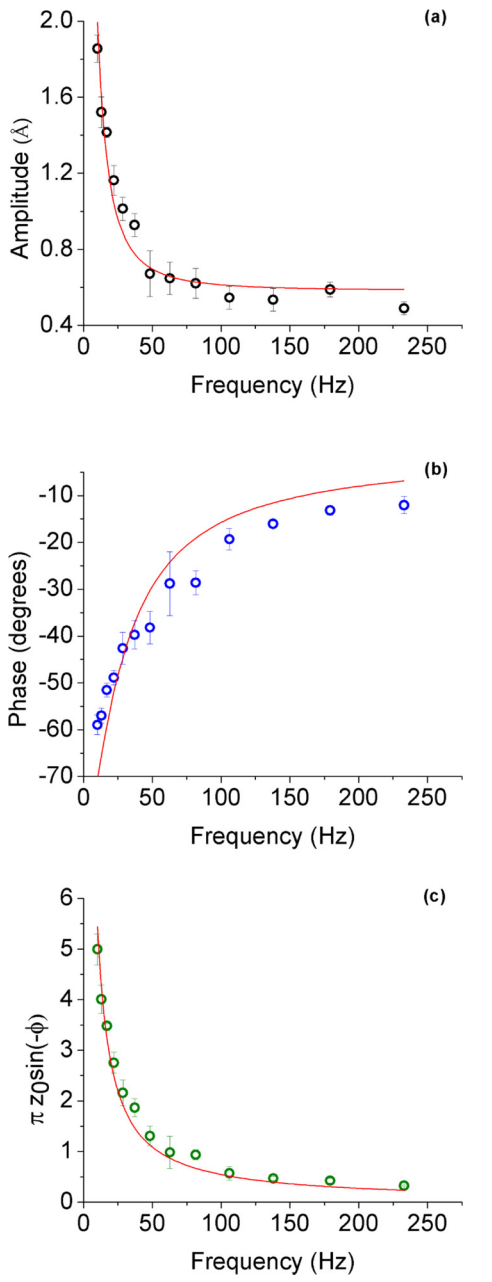

FIG. 6. Representative frequency scans for the mutant B1, arranged as in Fig. 5. The lines are fits with the Maxwell model [Eqs. (5) and (9)]. Mechanical differences between the mutants are not evident, but can be observed with sufficient averaging, as shown in Fig. 7.

$\omega_c = 170\,\text{rad/s}$ for Fig. 5 (mutant C1) and $\omega_c = 188\,\text{rad/s}$ for Fig. 6 (mutant B1). Comparing with the WT (Fig. 2), we do not see evident differences in the mechanics between the three molecules, by looking at individual samples. However, by averaging over several samples a trend emerges.

To better compare the mechanics of the three mutants we normalize all the data from all the mutants by dividing the amplitude of the response by the magnitude of the applied voltage for the corresponding sample. Then we take the average of all the data for each mutant and plot the average amplitude/voltage versus frequency. The result is shown in Fig. 7. With this normalization and averaging, some trend becomes observable, especially at higher frequencies. We see a departure from the Maxwell model behavior at high frequencies ($\omega \gg \omega_c$), in that the amplitude keeps decreasing with frequency. This effect is more pronounced for C1, compared to the WT. It is natural to associate this behavior with an additional mechanism for dissipation, not included in the Maxwell model. To quantify the different behavior of the mutants, we modify the Maxwell model Eq. (3) [which can be thought of as representing the dynamics of a spring (κ) and dashpot (γ_1) in series] by adding a second dashpot (γ_2) in parallel with the spring. We think of this

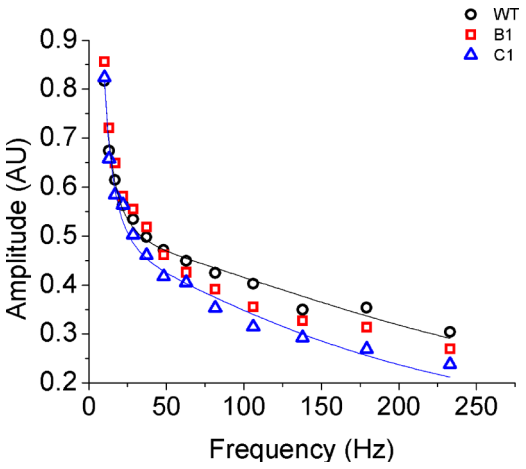

FIG. 7. Amplitude of the response for the WT (circles), B1 mutant (squares) and C1 mutant (triangles), averaged over several samples. The WT is averaged over five different samples, B1 over four, and C1 over three. There are systematic differences in the mechanics, especially between the WT and C1. Namely, in the region $\omega > \omega_c$ the amplitude for C1 decreases faster with frequency compared to the WT. Because this region is not captured well by the Maxwell model, we use a different form to fit the data (see text). Overall, the figure indicates that internal friction (as opposed to surface friction) is increased for C1.

addition as heuristically accounting for the internal dissipation of the molecule, while dissipation at the surface is accounted for by the dashpot in series with the spring. The equation of motion is now

$$\frac{\gamma_2}{\kappa}\ddot{x} + \dot{x} = \frac{F}{\gamma_1} + \frac{\dot{F}}{\kappa}\left(1 + \frac{\gamma_2}{\gamma_1}\right). \tag{11}$$

For an input $F(t) = F_0 e^{i\omega t}$, the amplitude of the response is

$$x_0(\omega) = \frac{F_0}{\omega\gamma_1}\frac{1}{\frac{\omega_c}{\omega} + r^2\frac{\omega}{\omega_c}}\sqrt{1 + \left(\frac{\omega_c}{\omega} + (r^2 + r)\frac{\omega}{\omega_c}\right)^2}, \tag{12}$$

where $\omega_c = \kappa/\gamma_1, r = \gamma_2/\gamma_1$, and to reiterate, we associate the dissipation constant γ_1 with the hydration layer, and γ_2 with the interior of the molecule. The lines in Fig. 7 are fits with Eq. (12), for the WT and C1 (the fit for B1 is not drawn for clarity, and because it is a poor fit). The result is that the difference in behavior between WT and fast (C1) mutant shown in Fig. 7 can be attributed to the internal dissipation described by γ_2, the fits returning the ratio $\gamma_2(C1)/\gamma_2(WT) = 1.4$. In summary, C1 has a higher "internal viscosity" compared to the WT.

We reported before that ligand binding to the enzyme carries a mechanical signature which can be detected by nanorheology [29]. Our next step was to probe whether this signature is different for the different mutants, potentially a "second order" mechanical effect. In the process of examining this question we also discovered that the amplitude and phase of the rheological response are complementary measurements with respect to detecting ligand binding, in the sense that in some cases, only the phase, in other cases, only the amplitude, shows a clear signature of ligand binding, in addition to cases where both phase and amplitude are affected.

Figure 8 shows, for the C1 mutant, experiments where the concentration of a ligand is varied while the amplitude and phase of the mechanical response is measured, at a fixed frequency $\nu = 12$ cycles/s (and fixed force amplitude). For GDP there is no clear mechanical signature of binding either in the amplitude in Fig. 8(a) or phase in Fig. 8(b). For ADP, the amplitude in Fig. 8(c) may show a small (∼0.1 Å!) increase upon binding, but the data are noisy. However, the phase in Fig. 8(d) shows a clean binding isotherm, increasing by ∼2 deg upon ADP binding. The line is a fit with the two-states binding isotherm,

$$f(C) = \alpha + \frac{\beta}{1 + K_d/C}, \tag{13}$$

where C is ligand concentration, returning the value $K_d^{\mathrm{ADP}}(C1) = 230\,\mu$M. For ATP, there is a clear signature in the amplitude in Fig. 8(e), which increases upon binding (i.e., the enzyme becomes floppier). The fit with Eq. (13) returns the value $K_d^{\mathrm{ATP}}(C1) = 1.2$ mM, exactly the same as our previous measurement on the WT [29], where we found $K_d^{\mathrm{ATP}}(\mathrm{WT}) = 1.2$ mM.

Figure 9 shows the amplitude and phase of the rheological response for different ligands binding to the WT. Similar to C1, GDP binding does not carry a clear mechanical signature either in the amplitude Fig. 9(a) or phase Fig. 9(b) (supposing, of course, that GDP does bind at concentrations <10 μM, which is the range explored in Figs. 8 and 9). Here too ADP binding is not very visible in the amplitude [Fig. 9(c)] but there is a clear signature in the phase Fig. 9(d). The fit with Eq. (13) gives $K_d^{\mathrm{ATP}}(\mathrm{WT}) = 240\,\mu$M, essentially the same as the value for C1.

In Fig. 10 we show the rheological response to GMP binding for B1 and C1. For B1, both amplitude Fig. 10(a) and phase Fig. 10(b) lead to well defined binding curves. The amplitude decreases by about 20% (or 0.4 Å working with ∼2 Å size deformations), and the phase decreases by ∼3 deg. The enzyme becomes stiffer upon binding GMP, as reported previously [6,29]. The lines are fits with Eq. (13), returning the values $K_d^{\mathrm{GMP}}(B1) = 5.7\,\mu$M from the amplitude measurements (a) and essentially the same value $K_d^{\mathrm{GMP}}(B1) = 4.6\,\mu$M from the phase measurements (b). The dissociation constant for the WT, which we reported previously [29], is the same: $K_d^{\mathrm{GMP}}(\mathrm{WT}) = 4.7\,\mu$M.

In contrast, the GMP binding curves for the fast mutant C1 show a new phenomenon. The amplitude Fig. 10(c) decreases in two steps, centered around [GMP] ≈ 5 μM and [GMP] ≈ 500 μM. This binding curve has been repeated a second time with an independent sample, and the same feature appears. We interpret this result as evidence that at high concentrations a second GMP molecule binds the enzyme, presumably occupying the ATP binding site. In this spirit, the line in Fig. 10(c) is a fit with a three-states binding equation,

$$f(C) = \alpha + \frac{\beta_1}{1 + K_d^{\mathrm{low}}/C} + \frac{\beta_2}{1 + K_d^{\mathrm{high}}/C}, \tag{14}$$

returning the values $K_d^{\text{low-GMP}}(C1) = 5.2\,\mu$M and $K_d^{\text{high-GMP}}(C1) = 620\,\mu$M. The lower binding constant is the same as for the B1 mutant and the WT. However, the phase

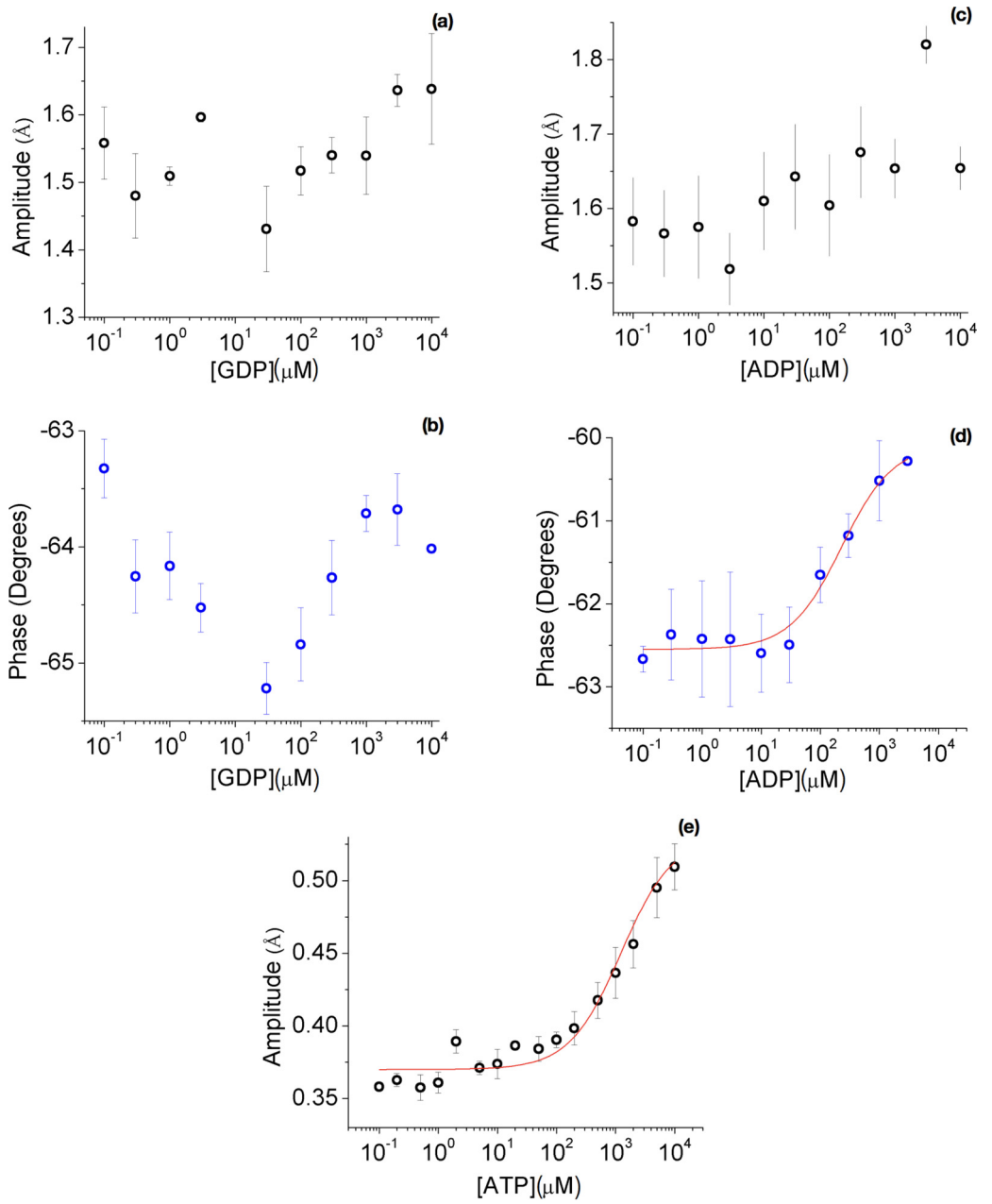

FIG. 8. Binding isotherms for GDP, ADP, ATP, measured by nanorheology for the "fast" mutant C1. Displayed are the amplitude and phase signals vs ligand concentration, measured at the the fixed frequency $\nu = 12$ Hz. For GDP, there is no signal above the scatter of the data, both for the amplitude (a) and the phase (b). For ADP, the amplitude signal (c) is unclear, whereas the phase (d) shows a clear signature of binding. The line is a fit with the two-states binding isotherm (13), yielding the dissociation constant $K_d^{\mathrm{ADP}}(C1) = 230\,\mu$M.(e) ATP binding curve obtained from the signal amplitude; the line is a fit with Eq. (13), yielding $K_d^{\mathrm{ATP}}(C1) = 1.2$ mM.

signal Fig. 10(d) is scattered, possibly due to the *collusion* of these two binding events.

III. DISCUSSION

By extending the measurements of the amplitude, which we reported previously, to measuring also the phase of the response function, we have shown that nanorheology enjoys the same features as a macroscopic rheology experiment, where one measures amplitude and phase, or equivalently, real and imaginary parts of the response function. The phase measurements were facilitated by the increase in sensitivity of the method obtained by making use of the plasmon resonance of the gold strip and gold nanoparticles in the detection optics [28,29]. Compared to evanescent wave scattering off resonance, the sensitivity is increased by a factor of about 6, and the signal over noise also improves because there is much more light [29]. With these technical improvements it also became clear that the amplitude versus frequency response (e.g., Fig. 7) is not quite a Maxwell model at high frequency ($\omega > \omega_c$): the amplitude keeps decreasing with frequency, signaling a dissipative contribution even in the "elastic" regime. We

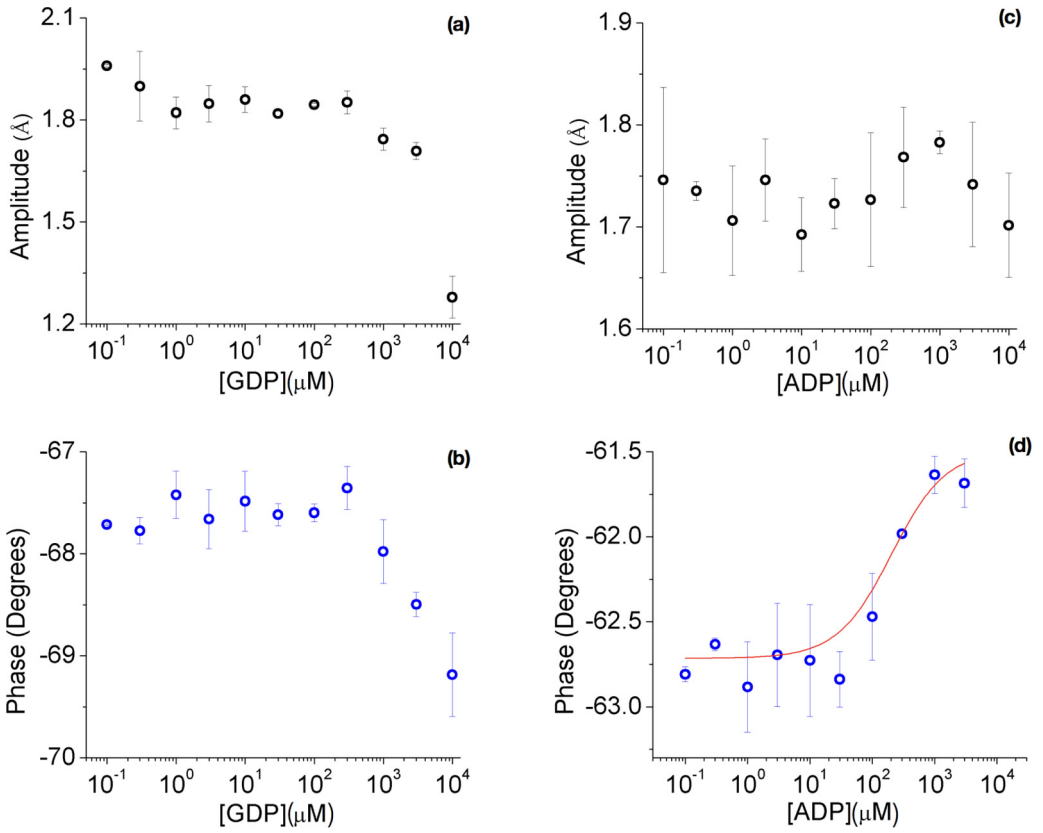

FIG. 9. Binding isotherms obtained by nanorheology for the WT. Similar to C1, there is no clear signature of GDP binding either in the amplitude (a) or phase (b) for concentrations [GDP] < 1 mM. The signature of ADP binding is not clear in the amplitude (c), but is visible in the phase (d). The line is a fit with Eq. (13), giving $K_d^{\mathrm{ADP}}(\mathrm{WT}) = 240\,\mu$M.

associate this contribution with the interior of the enzyme, because this is the feature in the response function that is different between the WT and the C1 mutant. However, we associate the parameter γ of the Maxwell model description Eq. (3) mostly with the surface of the enzyme, which includes the hydration layer, because we see this parameter change dramatically when we perturb the hydration layer with DMSO. The $1/\omega$ viscoelastic "divergence" of the response amplitude at low frequency is, however, associated with global deformations of the molecule, i.e., deformations of the surface and the interior: If we denature the protein, the response amplitude is feature-less [7].

For driven Å-size deformations, a large part of the dissipation comes from the hydration layer. This suggests to us that the same is probably true for large conformational motion driven by ligand binding (the induced fit mechanism [1]): In this case also the two interacting molecular surfaces (say GMP and the nucleotide binding site on GK) squeeze out the hydration layers to come into contact. For hard surfaces, the time course of this process has been beautifully measured by electron microscopy [9].

Substrate binding generally leads to a change in stiffness of the enzyme, which can be detected by nanorheology. Titrating in the ligand, one can obtain binding isotherms and measure the dissociation constant K_d; the value thus obtained is the same as that obtained by traditional spectroscopy with the molecule in solution, as shown in Ref. [29]. Here we have shown that both the amplitude and the phase may carry a signature of ligand binding. In different cases, one or the other may be more prominent, so for the determination of K_d it is helpful to have both measurements. The effect of ligand binding on the quantities directly measured by nanorheology is relatively small for the present system: $\sim$10% change in response amplitude, a few degrees change in the phase. Sub-Å resolution in the measurements is necessary to observe these changes. Keeping this in mind, the differences in the mechanical response observed between the WT and the two-Gly mutant (Fig. 7) appear the more significant. It is also noteworthy that ligand binding leads for some ligands to a stiffening of the structure, and for other ligands to a softening. For GK, binding of ATP and ADP makes the structure softer, while binding of GMP makes it stiffer. With GDP there is no clear signature. Looking overall at Figs. 8, 9, and 10, we find that when ligand binding leads to an increase in response amplitude, the phase also increases, while if the amplitude decreases, so does the phase. In terms of the viscoelastic description, it is easy to see from Eq. (5) that this means ligand binding affects primarily the elasticity parameter κ rather than the dissipation parameter γ. For example, from the data of Fig. 10(b) we get $\kappa_{\mathrm{GMP}}/\kappa_{\mathrm{apo}} = 1.14$ for B1. Of course, this specific value refers to the specific orientation of the molecule in the apparatus achieved in this experiment: The mechanical response of the enzyme is quantitatively different along different directions [35].

The C1 mutant is more resistive to driven deformations. This observation may support a recent evolutionary model

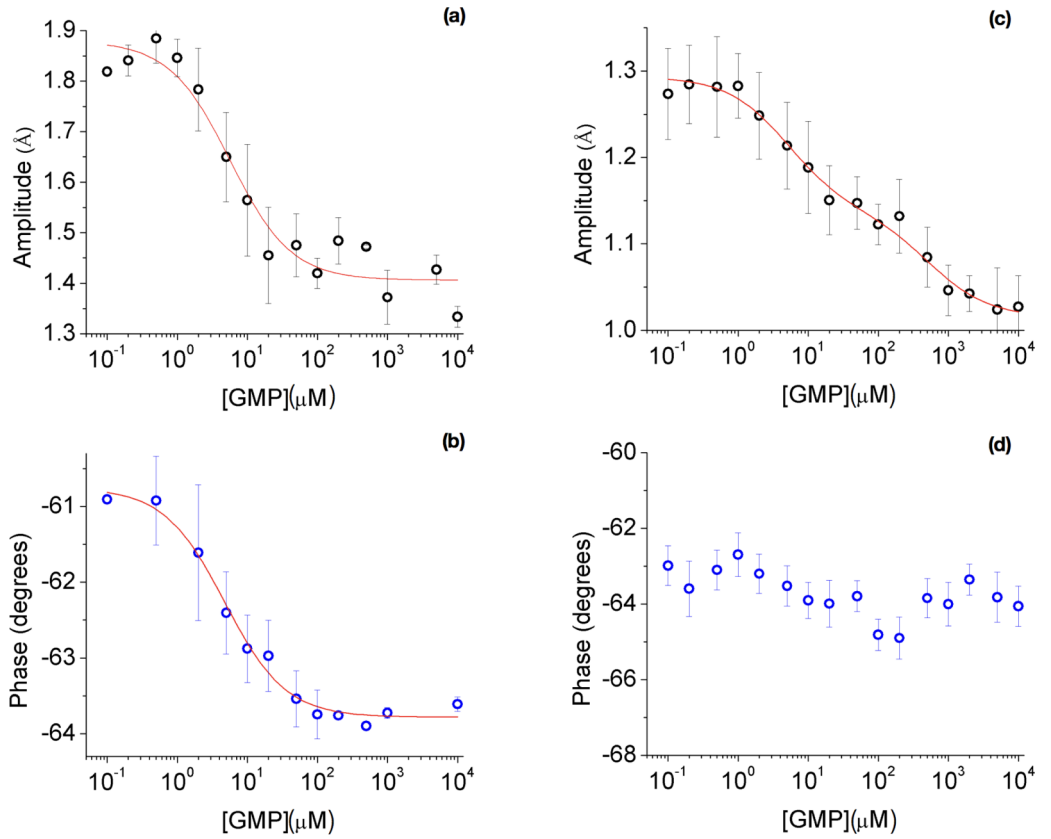

FIG. 10. GMP binding curves for B1 [(a) and (b)] and C1 [(c) and (d)]. Both mutants become stiffer upon binding GMP, as does the WT [29]. For B1, both the amplitude (a) and phase (b) carry a signature of GMP binding; fitting with Eq. (13) returns the values $K_d^{\mathrm{GMP}}(B1) = 5.7\,\mu$M from (a) and $K_d^{\mathrm{GMP}}(B1) = 4.6\,\mu$M from (b). (c) For C1, the GMP binding curve based on the amplitude shows two binding events, the first with midpoint [GMP] $\approx 5\,\mu$M and the second at [GMP] $\approx 600\,\mu$M. See text for more discussion. The line is a fit with Eq. (14).

of the emergence of allostery and global deformability as a percolation transition leading to an easily shearable plane in the interior of the enzyme [3]. In general, it may support the notion of an easily shearable channel spanning the molecule [24], which could be disrupted by point mutations. However, our results in this respect are quite preliminary, as we examined only two different mutants. To advance the understanding of this question, a more comprehensive study is needed, which is forthcoming [36].

What is the reason for the 10-fold differences in speed between B1, the WT, and C1? Figure 11 shows the molecular structure of GK, in open state [PDB: 1ZNW]. In this figure, the GMP binding domain is shown in red, ATP binding domain in violet, residues 075 and 171 (our two Cys handles) in cyan, residue 176 in blue, and residue 175 in green. The orange part is a water channel as defined in Ref. [37]. In the closed state, this water channel can potentially enable bound water molecules to interact with the enzymatic site, an interaction possibly crucial to the enzymatic activity [37]. This structure shows that our two mutation points are delicately located near this water channel. Considering that before mutation (in the WT) we had Ala in these two points, a hydrophobic amino acid, and in the mutants we have Gly, which is neither clearly hydrophobic nor hydrophilic, it is plausible that these mutations have altered the characteristic of the water channel. In C1, the *faster* mutant, the extra mutation point (residue 175 in green in Fig. 11) is right next to the water channel. This proximity can potentially bring some level of structure in the water molecules, in the closed state. Keeping in mind the importance of structured water molecules at the active site [37], having a more stable

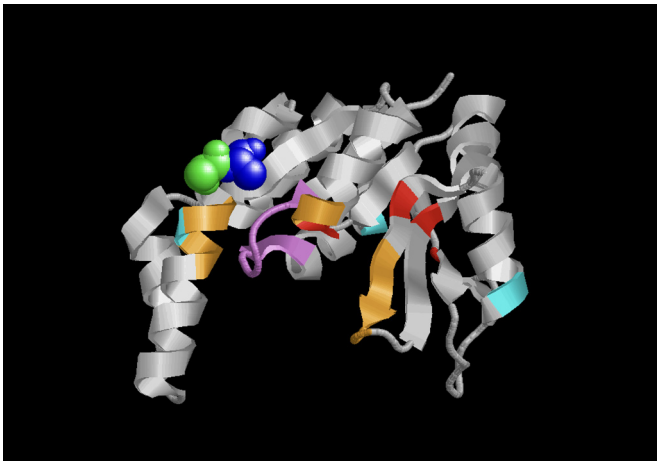

FIG. 11. Crystal structure of GK in open state from PDB 1ZNW. The GMP binding domain is shown in red, ATP binding domain in violet, residues 075, 171, and 042 in cyan, residue 176 in blue, and residue 175 in green. The orange part is a water channel as identified in Ref. [37].

closed state might result in a potential second binding site for GMP, as seen in Fig. 10(c).

Nanorheology may be at present the only method that probes global deformations of the whole system (polypeptide + hydration layer), at timescales comparable to the inverse rates of large conformational transitions (such as ligand-driven induced fit). We detect a dissipative process associated with global deformations driven by mechanical stress (Fig. 2), and we find that a large part of the dissipation originates in the hydration layer. If fluctuations in the hydration layer drive the equilibrium fluctuations of the system, as has been proposed [8,16,18,19], then dissipation must also occur primarily in the hydration layer. For Å-size, driven deformations at the frequencies of interest here, the magnitude of the dissipative energy per cycle is indeed of order the thermal energy. Using the last form in Eq. (8) with $\omega \approx \omega_c \Rightarrow \varphi \approx -\pi/4$, with $x_0 = 1$ Å and a plausible value $\kappa \sim 100$ pN/nm yields $W \sim 0.5$ kT (T being room temperature) for the energy dissipated per cycle. Since $\omega_c \approx 100$ rad/s, the corresponding value of the dissipation parameter is $\gamma = \kappa/\omega_c \approx 1$ pN · s/nm $= 1$ g/s, describing a very "viscous" nanometer-scale system [10].

As an incentive for future studies, we mentioned above that a wealth of insights has been obtained on enzyme dynamics through scattering experiments, which measure fluctuations. Nanorheology as presented here provides unique measurements of dissipation for the same systems. For a nanometer-scale system out of equilibrium, such as an enzyme or generally a molecular machine, the relation between nonlinearity, fluctuations, and dissipation is an important problem in nonequilibrium statistical mechanics [38,39].

IV. MATERIALS AND METHODS

Guanylate kinase (GK) from mycobacterium tuberculosis (gene Rv1389c) was modified by site-directed mutagenesis to remove the native cysteines from the wild type (substituted with Ser) and substitute two cysteines at sequence sites 75 and 171 for attachment to the gold surfaces. About half way through the experiments we realized that there is actually a third Cysteine (C3) in our gene, at position 042 (close to the position of one endogenous Cys which we removed, which is 040). It appeared surreptitiously during the mutagenesis process. Although the position of this third Cys is relatively buried, we may have a mixture of different orientations of the enzyme in the experiments. However, it turns out that the presence of Cys042 actually facilitates the experiments: when we removed the Cys042 again, we obtained a smaller coverage of GNPs on the slides and correspondingly smaller scattered intensity. Therefore, it was decided to continue the experiments with the three Cys molecules, since we do not have an *a priori* reason to prefer one or another orientation of the molecules in the apparatus. Expression and purification is described in Ref. [23]. Gold-coated slides and coverslips were made by evaporating a 3-nm layer of Cr followed by a 30-nm layer of gold using e-beam evaporator. In all the nanorheology experiments, the enzyme is in a saline sodium citrate buffer containing 50 mM sodium chloride and 5 mM trisodium citrate at pH = 7.0 (SSC/3). The chamber is illuminated by a He-Ne laser (632 nm), which is close to the SPR of the 30-nm gold layer. The SPR mode of the gold layer is excited, which in turn excites, in a distance-dependent manner, the plasmon resonance of the gold nanoparticles (also excited directly by the evanescent wave). The GNPs radiate with an intensity that, for small displacements, is proportional to their displacement with respect to the gold strip. The displacement calibration is described in Ref. [29]. Activities of the enzymes are measured with NADH assay, in which ADP and GDP production is coupled to two downstream reactions, resulting in the consumption of NADH. By measuring the decrease in the fluorescence of NADH, the activity of the enzyme is determined. For ligand-binding measurements, the response was measured at fixed voltage and frequency (∼300 mV and 12 Hz) first with no ligand present, then, for each point, exchanging the buffer in the chamber with the same buffer containing the specified concentration of ligand.

ACKNOWLEDGMENTS

We gratefully acknowledge support from the NSF under Grant No. DMR-1404400. We thank Tsvi Tlusty, Elisha Moses, and Chiao-Yu Tseng for essential discussions and encouragement, and Chiao-Yu Tseng and Tsvi Tlusty for generating Fig. 3.

[1] D. E. Koshland, The key-lock theory and the induced fit theory, Angew. Chem. Int. Ed. Engl. **33**, 2375 (1994).

[2] P. Maragakis and M. Karplus, Large amplitude conformational change in proteins explored with a plastic network model: Adenylate Kinase, J. Mol. Biol. **352**, 807 (2005).

[3] T. Tlusty, A. Libchaber, and J.-P. Eckmann, Physical Model of the Genotype-to-Phenotype Map of Proteins, Phys. Rev. X **7**, 021037 (2017).

[4] G. Zocchi, Controlling proteins through molecular springs, Ann. Rev. Biophys. **38**, 75 (2009).

[5] C.-Y. Tseng and G. Zocchi, Mechanical control of renilla luciferase, J. Am. Chem. Soc. **135**, 11879 (2013).

[6] Y. Wang and G. Zocchi, Elasticity of Globular Proteins Measured from the AC Susceptibility, Phys. Rev. Lett. **105**, 238104 (2010).

[7] A. Ariyaratne, C. Wu, C.-Y. Tseng, and G. Zocchi, Dissipative dynamics of enzymes, Phys. Rev. Lett. **113**, 198101 (2014).

[8] H. Frauenfelder *et al.*, A unified model of protein dynamics, Proc. Natl. Acad. Sci. USA **106**, 5129 (2005).

[9] U. Anand, J. Lu, D. Loh, Z. Aabdin, and U. Mirsaidov, Hydration layer-mediated pairwise interaction of nanoparticles, Nano Lett. **16**, 786 (2016).

[10] Y. Wang and G. Zocchi, The folded protein as a viscoelastic solid, Europhys. Lett. **96**, 18003 (2011).

[11] H. Qu, J. Landy, and G. Zocchi, Cracking phase diagram for the dynamics of an enzyme, Phys. Rev. E **86**, 041915 (2012).
[12] Y. Wang and G. Zocchi, Viscoelastic transition and yield strain of the folded protein, PLoS ONE **6**, e28097 (2011).
[13] H. Qu and G. Zocchi, How Enzymes Work: A Look through the Perspective of Molecular Viscoelastic Properties, Phys. Rev. X **3**, 011009 (2013).
[14] C. Fogle, J. Rudnick, and D. Jasnow, Protein viscoelastic dynamics: A model system, Phys. Rev. E **92**, 032719 (2015).
[15] B. H. McMahon, F. G. Parak, P. W. Fenimore, and H. Frauenfelder, Slaving: Solvent fluctuations dominate protein dynamics and functions, Proc. Natl. Acad. Sci. USA **99**, 16047 (2002).
[16] B. H. McMahon, R. D. Young, P. W. Fenimore, and H. Frauenfelder, Bulk-solvent and hydration-shell fluctuations, similar to α and β fluctuations in glasses, control protein motions and functions, Proc. Natl. Acad. Sci. USA **101**, 14408 (2004).
[17] G. Chen, B. H. McMahon, H. Frauenfelder, and P. W. Fenimore, Protein folding is slaved to solvent motions, Proc. Natl. Acad. Sci. USA **103**, 15469 (2006).
[18] L. Wanga, Y. Qina, and D. Zhong, Dynamics and mechanism of ultrafast water-protein interactions, Proc. Natl. Acad. Sci. USA **113**, 8424 (2016).
[19] J. Yang, Y. Wang, L. Wang, and D. Zhong, Mapping hydration dynamics around a β-barrel protein, J. Am. Chem. Soc. **139**, 4399 (2017).
[20] C. Lopez, D. A. Wesener, W. Hubbell, S. Cavagnero, B. D. Armstrong, J. Choi, and S. Han, Site-specific hydration dynamics in the nonpolar core of a molten globule by dynamic nuclear polarization of water, J. Am. Chem. Soc. **133**, 5987 (2011).
[21] E. Persson and B. Halle, Cell water dynamics on multiple timescales, Proc. Natl. Acad. Sci. USA **105**, 6266 (2008).
[22] J. A. Scott, J. M. Franck, and S. Han, Nonlinear scaling of surface water diffusion with bulk water viscosity of crowded solutions, J. Am. Chem. Soc. **135**, 4175 (2013).
[23] Z. Alavi, A. Ariyaratne, and G. Zocchi, Nano-rheology measurements reveal that the hydration layer of enzymes partially controls conformational dynamics, Appl. Phys. Lett. **106**, 203702 (2015).
[24] T. Tlusty, M. R. Mitchell, and S. Leibler, Strain analysis of protein structures and low dimensionality of mechanical allosteric couplings, Proc. Natl. Acad. Sci. USA **113**, E5847 (2016).
[25] Y. Savir and T. Tlusty, Conformational proofreading: The impact of conformational changes on the specificity of molecular recognition, PLoS ONE **2**, e468 (2007).
[26] R. M. Y. Savir, E. Noor, and T. Tlusty, Cross-species analysis traces adaptation of rubisco toward optimality in a low-dimensional landscape, Proc. Natl. Acad. Sci. USA **107**, 3475 (2010).
[27] H. Jensenius and G. Zocchi, Measuring the Spring Constant of a Single Polymer Chain, Phys. Rev. Lett. **79**, 5030 (1997).
[28] J. J. Mock, R. T. Hill, Y.-J. Tsai, A. Chilkoti, and D. R. Smith, Probind dynamically tunable localized surface plasmon resonances of film-coupled nanoparticles by evanescent wave excitation, Nano Lett. **12**, 1757 (2012).
[29] A. Ariyaratne and G. Zocchi, Plasmon resonance enhanced mechanical detection of ligand binding, Appl. Phys. Lett. **106**, 013702 (2015).
[30] I. I. Vaismant and M. L. Berkowitz, Local structural order and molecular associations in water-DMSO mixtures. Molecular dynamics study, J. Am. Chem. Soc. **114**, 7889 (1992).
[31] D. Russo, The impact of kosmotropes and chaotropes on bulk and hydration shell water dynamics in a model peptide solution, Chem. Phys. **345**, 200 (2008).
[32] B. Jana, S. Roy, and B. Bagchi, Dimethyl sulfoxide induced structural transformations and nonmonotonic concentration dependence of conformational fluctuation around active site of lysozyme, J. Chem. Phys. **136**, 115103 (2012).
[33] P. Christova, L. Renault, E. Seclaman, A. Thompson, E. Girard, H. Munier-Lehmann, J. Cherfils, and G. Hible, Unique gmp-binding site in mycobacterium tuberculosis guanosine monophosphate kinase, Proteins **62**, 489 (2006).
[34] D. Dreusike and G. E. Schulz, The glycine-rich loop of adenylate kinase forms a giant anion hole, FEBS Lett. **208**, 301 (1986).
[35] C.-Y. Tseng, A. Wang, and G. Zocchi, Mechano-chemistry of the enyzme guanylate kinase, Europhys. Lett. **91**, 18005 (2010).
[36] Elisha Moses (private communication).
[37] S. Sacquin-Mora, O. Delalande, and M. Baaden, Enzyme closure and nucleotide binding structurally lock guanylate kinase, Biophys. J. **101**, 1440 (2011).
[38] H. Qian, Cooperativity in cellular biochemical processes: Noise-enhanced sensitivity, fluctuating enzyme, bistability with nonlinear feedback, and other mechanisms for sigmoidal responses, Annu. Rev. Biophys. **41**, 179 (2012).
[39] A. B. Kolomeisky, H. Qian, S. Kjelstrup, and D. Bedeaux, Entropy production in mesoscopic stochastic thermodynamics: Nonequilibrium kinetic cycles driven by chemical potentials, temperatures, and mechanical forces, J. Phys.: Condens. Matter **28**, 153004 (2016).